

Biped Gait Controller for Large Speed Variations, Combining Reflexes and a Central Pattern Generator in a Neuromuscular Model

Nicolas Van der Noot^{1,2}, Auke J. Ijspeert² and Renaud Ronsse¹

Abstract—Controllers based on neuromuscular models hold the promise of energy-efficient and human-like walkers. However, most of them rely on optimizations or cumbersome hand-tuning to find controller parameters which, in turn, are usually working for a specific gait or forward speed only. Consequently, designing neuromuscular controllers for a large variety of gaits is usually challenging and highly sensitive. In this contribution, we propose a neuromuscular controller combining reflexes and a central pattern generator able to generate gaits across a large range of speeds, within a single optimization. Applying this controller to the model of COMAN, a 95 cm tall humanoid robot, we were able to get energy-efficient gaits ranging from 0.4 m/s to 0.9 m/s. This covers normal human walking speeds once scaled to the robot height. In the proposed controller, the robot speed could be continuously commanded within this range by changing three high-level parameters as linear functions of the target speed. This allowed large speed transitions with no additional tuning. By combining reflexes and a central pattern generator, this approach can also predict when the next strike will occur and modulate the step length to step over a hole.

I. INTRODUCTION

Dynamic walking gaits with a robot can be achieved using many approaches. Among them, those relying on the zero-moment point (ZMP), an indicator of dynamic stability [1], are likely the most famous ones. Using this framework, humanoid robots like ASIMO [2] or HRP-2 [3] perform robust gaits. However, controllers based on these approaches usually present some limitations like energy-inefficiency, high computational cost and non human-like features like continuous knee bending [4]-[5].

In parallel, some models consider the human gait as a limit cycle and focus on global stability. This leads to the concept of *limit cycle walking* [6]. Among these, the neuromusculoskeletal model developed by Geyer and Herr [7] relies on reflex-based controlled muscles generating torques at the joint level. Interestingly, this approach can generate robust and energy-efficient gaits similar to the human ones in terms of muscles activities, joint angles and torques.

The reflex rules developed in [7] require an optimization phase (or manual tuning) of the many open parameters

governing the contribution of each local reflex. This approach makes the optimized parameters set working for a single gait speed. When the robot is walking, it is thus not easy to change its speed or its stride length.

A first strategy to overcome this limitation was developed by Song and Geyer [8]. It consists in optimizing different gaits and then modulating some key control parameters to change the forward speed during the walking gait. However, this approach can only cope with small speed changes after a first optimization. High speed variations require then running extra optimizations to find new parameter modulations between pre-optimized walking gaits.

Another approach developed by Dzeladini et al. [9] introduces a central pattern generator (CPG), a neural circuit capable of producing rhythmic neural activity patterns without receiving rhythmic inputs [10]. The CPG is used as a feed-back predictor of the reflex rules from [7]. This CPG can thus be used as a feed-forward component, reducing the complexity in the speed control strategy of [8]. Nevertheless, this approach requires to capture (with third order spline interpolations) the reflex rules outputs that were optimized for one precise walking speed with no feed-forward contribution. Consequently, the gait is not optimal (regarding energy-efficiency) for the whole range of speeds. On top of that, this leads to a speed transition range being smaller than the one from [8].

In this contribution, we also propose a controller mixing reflexes and a CPG to control the leg muscles. Our CPG is designed as a six-neurons network of Matsuoka oscillators [11]-[12] sending feed-forward signals to the proximal muscles controlling the hip. These bio-inspired artificial oscillators, capturing the mutual inhibition between half-centers located in the spinal chord, are widely used to model the firing rate of mutually inhibiting neurons, in both the upper and the lower extremities [13].

The controller can then be optimized for a large range of walking speeds, co-optimizing reflexes and CPG parameters at the same time within a single optimization. We applied this approach to a simulation of the COMAN, a humanoid robot presented in section II. Then, in section III, we detail the controller itself and the associated optimization process, while section IV presents the strategy used to adapt the robot speed during the walking gait. Section V analyses the resulting gaits, comparing them to the ones obtained with the original model of [7]. Results about speed transitions, strike prediction and holes stepping techniques are also presented. Finally, we conclude the paper in section VI.

This work was supported by the Belgian F.R.S.-FNRS (Aspirant #16744574 awarded to NVdN, Cr dit aux Chercheurs #6809010 awarded to RR) and by the European Community's Seventh Framework Programme under Grant 611832 (WALK-MAN) and Grant 611626 (SYMBITRON).

¹N. Van der Noot and R. Ronsse are with the Center for Research in Energy and Mechatronics, Institute of Mechanics, Materials and Civil Engineering, Universit  catholique de Louvain, B-1348 Louvain-la-Neuve, Belgium.

²N. Van der Noot and A. J. Ijspeert are with The Biorobotics Laboratory, School of Engineering, Institute of Bioengineering,  cole Polytechnique F d rale de Lausanne, CH-1015 Lausanne, Switzerland.

II. COMAN PLATFORM

We use a simulation model of the 95 cm tall COMpliant HuMANoid platform (COMAN). This robot, developed by the Italian Institute of Technology (IIT), has 23 actuated degrees of freedom (DOFs), most of them being equipped with series elastic actuators [14]. Each joint is equipped with position, velocity and torque sensors. The robot also features an inertial measurement unit (IMU) and 6-DOF feet force and torque sensors measuring ground reactions. Our controller only uses sensory inputs available on this robot. Further information can be found in [15] and [16].

The COMAN (visible in Fig. 1b) is modelled in a simulation environment called Robotran [17]. Its actuators implementation is described in [15]. In this contribution, we artificially constrain the waist to stay in the world sagittal plane to study 2D walking gaits only.

III. CONTROLLER DESIGN

The purpose of our controller is to produce position or torque references for each of the 23 DOFs of the robot. We briefly describe the control rules for the main of them before focussing on the three sagittal joints of each leg.

A. Joints control

The COMAN has eleven DOFs for the upper body: three in the torso and four per arm. All torso joints are controlled to track zero position. For arms control, we use similar rules as the ones presented in [18]. In short, constant position references are tracked for the elbow sagittal DOF (0.25 rad), the shoulder lateral DOF (0.09 rad) and the shoulder transverse DOF (0.14 rad). Finally, the shoulder sagittal DOF ϕ_s^s tracks a linear function of the hip angles difference as $\phi_s^s = 0.3 * (\theta_h^R - \theta_h^L) - 0.3$ where θ_h^R and θ_h^L are the right and left sagittal hip positions (θ_h^R and θ_h^L are inverted for the left shoulder), all expressed in radians. Such control leads to balancing arm trajectories reducing the total energy consumption during the walking gait [18].

Regarding the lower body, each leg has three sagittal DOFs, two lateral DOFs and one transverse DOF. All leg non-sagittal joints track zero position, to comply with the 2D walking. Finally, the three sagittal joints, being the main focus of this contribution, rely on the neuromuscular model controller described in sections III-B to III-E. The initial posture of the robot constraints all joints to track zero position which corresponds to an upright posture, except the sagittal ankle tracking a position κ to be optimized (see Table I).

B. Musculoskeletal model

We focus here on the leg sagittal DOFs which are the most important joints propelling the body forward. The model proposed by Geyer and Herr [7] actuates each leg with seven Hill-type muscles, capturing the contribution of the main muscle groups of the human leg. For our COMAN model, these virtual muscles are depicted in red in Fig. 1b, producing torque references in a way similar to [7]. The key idea is the following: muscles react by contracting and apply forces on

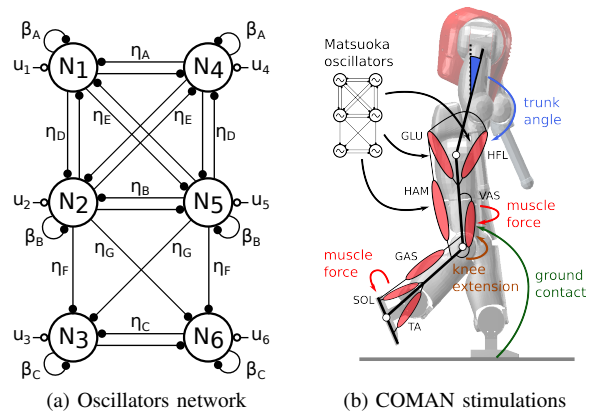


Fig. 1: The six-neurons oscillators network sends stimulations to the proximal muscles, while the distal ones are only driven by reflexes. The hip flexor muscles (HFL) are stimulated by both the CPG and the reflexes.

the body. Therefore, the equivalent torques applied by the seven muscles on the leg sagittal joints are computed from the segments free-body diagrams. These torque references are sent to a PI controller feeding the actuators (implemented like in [15]). Their state computation is fully described in [7] and [19]. The main muscle properties are scaled to fit the size and the weight of the COMAN, using dynamic scaling [20].

Each muscle is then controlled by its activation $A(t)$, capturing the neural signal provided by motoneurons. This signal is related to a neural input $S(t)$, the muscle stimulation, using a first-order low-pass filter capturing the excitation-contraction coupling [19]. Controlling the muscle model thus reduces to designing control rules for the stimulations $S(t)$ driving the seven muscle groups of each leg.

C. Central pattern generator design

Central pattern generators (CPGs) are neural circuits capable of producing rhythmic patterns of neural activity without receiving rhythmic inputs [10]. They present attractive properties like distributed control, redundancies handling, and locomotion modulation using simple control signals [10]. While locomotor CPGs have been identified in many vertebrates, their recruitment for human locomotion is still a matter open to discussion [21]. Yet, computational models show that CPGs could play a major role in human locomotion. For instance, Taga et al. [22] demonstrated bipedal locomotion ability to adapt to a changing environment using CPG modulations. The work of Paul et al. [23] proposed a neuro-musculo-skeletal model studying the effects of spinal cord injury on locomotor abilities, again with a CPG as central element.

In this contribution, a CPG structure is used to send descending feed-forward signals to proximal muscles, i.e. muscles driving the hip joint. This is coherent with the *proximo-distal gradient* hypothesis postulating that CPGs mostly drive the proximal muscles while the distal ones should be driven by reflexes [9]. Indeed, distal muscles are

more impacted by external perturbations like ground interactions [24]. The three proximal muscle groups controlled by the CPG are the hip flexors (HFL), the gluteus muscle group (GLU) and the biarticular hamstring muscle group (HAM), presented in Fig. 1b.

The firing rate x_i of each neuron N_i is computed according to Eq. (1) where v_i is the self-inhibition modulated by an adaptation constant β_j , u_i the external excitation and τ is a time constant. The connexion strengths η_k tune the mutual inhibitions. The $[\bullet]^+$ function takes the positive part of its argument (it saturates to zero when the argument is negative) and thus captures the fact that the activation of a given neuron decreases when another is active (mutual inhibition). Fig. 1a depicts the Matsuoka network with six neurons N_i that is used to drive these virtual muscles, along with the parameters β_j , u_i and η_k .

$$\dot{x}_i = \frac{1}{\tau}(-x_i - \beta_j v_i - \sum_1^3 \eta_k [x_l]^+ + u_i) \quad (1)$$

The self-inhibition computation is captured by Eq. (2) where γ_j is a constant multiplying τ . The index i corresponds to the neuron index, while the indexes k and l in Eq. (1) are replaced according to Fig. 1a. Index j equals A for neurons N_1 and N_4 , B for N_2 and N_5 and C for N_3 and N_6 . These rules are fully developed in Appendix A.

$$\dot{v}_i = \frac{1}{\gamma_j \tau}(-v_i + [x_i]^+) \quad (2)$$

This network obeys a mirror symmetry due to the symmetry of the right and left leg. This symmetry between neurons N_1, N_2, N_3 and neurons N_4, N_5, N_6 can be observed in the mutual inhibition connexions strength η_k in Fig. 1a and also in the full equations development provided in Appendix A.

Neurons N_1, N_2, N_4 and N_5 form a fully-connected network where each neuron fires alternatively over the cycle. These neurons will stimulate the HAM and GLU muscles of each leg. Neurons N_3 and N_6 receive inputs from them but do not interfere on this first fully-connected network. In this way, their respective own parameters β_j , γ_j and η_k provide more flexibility to stimulate the HFL muscles.

Similarly to [23], this CPG can also be modulated by the interactions between the robot body and its environment. This is done via short excitations modulations at foot strike. The input excitations u_i of the neurons first consist in a tonic excitation equal to u . For simplicity, this tonic contribution is kept equal to 1. Modulations of the oscillators output will rather be governed by external gains (see Eq. (5)). Some terms are further added to the excitation component in order to achieve synchronization between the oscillators and the walking gait. In particular, the firing rate x_1 is expected to switch from a negative to a positive value at the moment of right foot strike. Similarly, x_4 is expected to become positive at left foot strike.

This results in Eq. (3). The function $[\bullet]^-$ takes the absolute value of its argument if it is negative, and saturates to zero otherwise. On top of that, the function $[\bullet]_{SR}$ keeps its

argument intact during the right leg supporting phase, while saturating it to zero otherwise (similar for the left leg with $[\bullet]_{SL}$). Then, $[\bullet]_{Str,R}$ always saturates its argument to zero, except after the right foot strike if the firing rate x_1 is still negative. In this case, it keeps its argument intact as long as x_1 is negative (similar for $[\bullet]_{Str,L}$ with the left leg and x_4). Finally, the excitation u_i of all neurons is forced to zero when x_1 becomes positive before right strike or when x_4 becomes positive before left strike, again in order to achieve the desired synchronization.

$$\begin{aligned} u_1 &= u - [x_1]_{SL}^+ + [x_1]_{Str,R}^- & u_4 &= u - [x_4]_{SR}^+ + [x_4]_{Str,L}^- \\ u_2 &= u - [x_2]_{SL}^+ - [x_2]_{Str,L}^+ & u_5 &= u - [x_5]_{SR}^+ - [x_5]_{Str,R}^+ \\ u_3 &= u - [x_3]_{SL}^+ & u_6 &= u - [x_6]_{SR}^+ \end{aligned} \quad (3)$$

The terms $-[\bullet]_{SR/SL}^+$ are used to make each neuron firing rate synchronizing with the appropriate leg. In steady-state, this term is thus always zero. The terms $\pm[\bullet]_{Str,R/L}^\mp$ are used when the oscillators are too slow. Then, a burst is provided to the late neurons while others are partially inhibited. On the contrary, if the oscillators are faster than requested, all excitations are forced to zero so that all firing rates will slowly converge to zero. Again, in steady-state, the contribution of these synchronization terms is very limited. These mechanisms achieve the synchronization between the different neurons. Interestingly, these synchronization mechanisms make the oscillators able to predict when the next strike will happen. Some associated results are presented in section V-D. Walk initiation is simply achieved by sending an excitation of 1 to two neurons (N_1, N_3 or N_4, N_6) while the other excitations are set to zero. After 0.2 s, all excitations are activated, as previously explained.

Finally, the oscillators produce four outputs y_i , taken as the difference between the positive part of the firing rates x_i of two adjacent neurons, see Eq. (4). This arrangement is designed to feed the appropriate signals to the different muscles during the different walk phases (e.g. high stimulations to the HFL muscles during early swing to flex the corresponding hip), see Eq. (5).

$$\begin{aligned} y_1 &= [x_1]^+ - [x_2]^+ & y_3 &= [x_4]^+ - [x_5]^+ \\ y_2 &= [x_3]^+ - [x_2]^+ & y_4 &= [x_6]^+ - [x_5]^+ \end{aligned} \quad (4)$$

D. Muscle stimulations

Muscles stimulations are computed as combinations of CPG output signals y_i , reflex rules and prestimulations S_0 . This combination is presented in Fig. 1b. The stimulations are all bounded between 0.01 and 1. All the reflex rules are adapted from [7]. However, using oscillators to feed the proximal muscles allows to drastically reduce the number of reflex rules.

The stimulations of the three proximal muscle groups HFL, GLU and HAM, respectively $S_{HFL,R/L}$, $S_{GLU,R/L}$ and $S_{HAM,R/L}$ for the right/left leg are linear combinations of the CPG output signals y_i positive part, see Eq. (5). k_{HFL} , k_{GLU} , $k_{HAM,1}$ and $k_{HAM,2}$ are four gains presented in Appendix C.

$$\begin{aligned}
S_{HFL,R} &= k_{HFL} [y4]^+ & S_{HFL,L} &= k_{HFL} [y2]^+ \\
S_{GLU,R} &= k_{GLU} [y1]^+ & S_{GLU,L} &= k_{GLU} [y3]^+ \\
S_{HAM,R} &= k_{HAM,1} [y1]^+ + k_{HAM,2} [y3]^+ \\
S_{HAM,L} &= k_{HAM,1} [y3]^+ + k_{HAM,2} [y1]^+
\end{aligned} \tag{5}$$

On top of that, the HFL muscles receive an extra stimulation S_{HFL}^{ext} coming from [7] to help maintaining the trunk to a desired reference position θ_{ref} (in radians):

$$S_{HFL}^{ext} = \xi_1 \frac{F_z}{w} (\theta_{ref} - \theta_t - \xi_2 \dot{\theta}_t) \tag{6}$$

where θ_{ref} , ξ_1 and ξ_2 are three parameters to be optimized, θ_t is the trunk absolute angle, $\dot{\theta}_t$ its derivative, w the whole robot weight and F_z the vertical force under the foot of the corresponding leg. This extra stimulation is a reflex similar to a PD controller stabilizing an inverted pendulum.

Two muscle groups only receive a constant prestimulation S_0 : the gastrocnemius (GAS) and the tibialis anterior (TA). S_0 is put to 0.01 (the minimal stimulation). Finally, the vasti muscles (VAS) and the soleus muscles (SOL) receive only the prestimulation during swing, while receiving positive force feed-back reflexes during stance [7]:

$$\begin{aligned}
S_{VAS} &= S_{0,VAS} + G_{VAS} (F_{VAS}/F_{VAS,max}) \\
S_{SOL} &= S_0 + G_{SOL} (F_{SOL}/F_{SOL,max})
\end{aligned} \tag{7}$$

where G_{VAS} and G_{SOL} are two parameters to be optimized, $F_{VAS}/F_{VAS,max}$ and $F_{SOL}/F_{SOL,max}$ are the normalized forces produced by these two muscles and $S_{0,VAS}$ is the prestimulation of the VAS muscle, which is optimized and can exceed 0.01. Finally, S_{VAS} is set to $S_{0,VAS}$ when the corresponding leg is the trailing leg during the double support phase or if the corresponding knee angle ϕ_k exceeds an over-extension threshold ϕ_{off} (to be optimized) while $\dot{\phi}_k$ is positive (see [7]). This prevents knee over-extension.

E. Optimization of the gait controller

We use a particle swarm optimization (PSO) algorithm to optimize the open parameters [25]. These parameters are listed in Appendix B, Table I, along with their bounds. All optimization runs simulate a 60 s walking gait. To encourage solutions with enough foot clearance with the ground, obstacles are added below the swing foot during optimization. These bumps are trapezoidal shapes placed next to the foot in contact with the ground. Their height linearly increases with the simulation time from 0 cm to 3 cm. The objective function used to evaluate each set of parameters is staged in the sense that different objectives are sorted by order of relevance, such that the next objective is taken into account only when the previous one is fulfilled.

The first stage requires the robot to walk without falling during the 60 s simulation time, the fitness being proportional to the walking time. When this objective is reached, the speed is later optimized to match a target speed. The corresponding objective function is given in Eq. (8), where f is the objective function, x the parameter to be constrained (the speed here), x^* is the target parameter and α , β are two weight parameters. This output is then bounded between 0 and α . When

the robot speed is in a range of 0.05 m/s around the target speed, the last fitness stage is triggered. There, we minimize the metabolic energy consumption in muscle contraction per unit distance walked [26] and the oscillators prediction error, summing their corresponding objective functions. Indeed, a good oscillator phase prediction is potentially relevant to develop other mechanisms requiring gait synchronization, see section V-D. In both cases, we also use Eq. (8) where x now represents the metabolic energy consumption per unit distance walked or the time error between the oscillator strike prediction and the actual one. In both cases, the target x^* is equal to zero, since the objective is to minimize both the energy consumption and the prediction error.

$$f = \alpha e^{-\beta(x-x^*)^2} \tag{8}$$

IV. SPEED ADAPTATION

In this section, the controller is further extended with the objective to optimize several gaits (corresponding to a range of different speeds) within a single optimization. This will allow the modulation of speed when the robot is walking. This speed modulation is mainly performed by adapting two features of the CPG: frequency and amplitude. Indeed, faster walking speeds usually correspond to faster walking frequencies and longer step lengths [27]. Moreover, faster speeds result in larger trunk tilt, as identified in [8]. Consequently, the trunk angle reference θ_{ref} acting on the HFL muscles also needs to be adapted as a function of the desired speed, θ_{ref} increasing for faster gaits. The oscillators frequency is tuned with the time constant τ , decreasing with higher speeds. To modify the oscillators outputs amplitude, we adapt the gains k_{HFL} , k_{GLU} , $k_{HAM,1}$ and $k_{HAM,2}$, using different adaptation laws for each of them. Indeed, an increase in speed does not necessary result in an uniform scaling of the muscles stimulations. In this case, it is less trivial to predict how these parameters will evolve with the robot speed.

The evolutions of these three types of parameters is studied in section V-A. It appears that they can be approximated by linear functions of the target speed, according to the rules described in Appendix C, which are used to extend our controller to speed adaptation. So, the strategy is the following. The optimization process always targets an arbitrary speed of 0.6 m/s for initiation. After four steps, the speed parameters are updated for a new target speed according to the rules described in Appendix C. Each set of optimized parameters is then tested for a large range of different speeds, and the objective function is set as the average of each trial. In this way, we co-optimize all parameters for the largest possible range of speeds (from 0.4 m/s to 0.9 m/s).

V. RESULTS

The CPG-based controller presented in this paper is compared with the reflex-based approach from [7]. To this end, we first study the evolution of the parameters presented in section IV. We also present the ability of our CPG-based controller to track a speed reference, to predict when the next strike will happen and to step over holes.

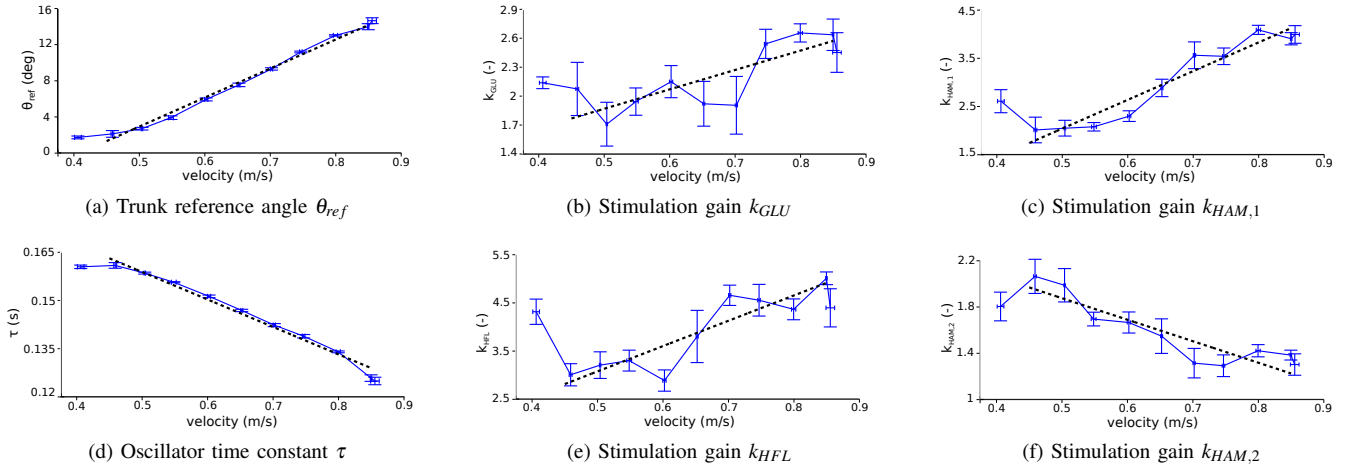


Fig. 2: We run five optimizations for each target speed and we measure the actual speed of each solution, along with the optimized value of the six open parameters. For each target speed, we gather the five optimization final results, presenting their mean and standard deviations. For graph legibility, the errorbars represent half of the standard deviations. Dashed lines present the linear approximations for the range of speeds between 0.45 m/s and 0.85 m/s, using the minimum mean square error method.

A. Speed parameters

Six parameters were identified in section IV to be adapted as a function of the walking speed (θ_{ref} , τ , k_{GLU} , k_{HFL} , $k_{HAM,1}$ and $k_{HAM,2}$). First, an optimization with an arbitrary target speed of 0.6 m/s is launched. Then, all the optimized parameters are frozen, except the six parameters being left for speed adaptation. New optimizations were then performed, allowing only these six parameters to change across the different target speeds. Our target speed experiments run from 0.4 m/s to 0.9 m/s with a 0.05 m/s step. We run five optimizations for each target speed and report the evolution of the six parameters in Fig. 2.

Let's first take a look at the speeds ranging from 0.45 m/s to 0.85 m/s. There, the evolution of θ_{ref} and τ can be captured by linear functions of the speed. On top of that, this matches the expectations: θ_{ref} increases with speed while τ decreases. Similar observations can be performed for the amplitude gains: k_{GLU} and $k_{HAM,1}$ impact the stance phase while k_{HFL} and $k_{HAM,2}$ impact the swing phase. During stance phase, k_{GLU} and $k_{HAM,1}$ are both used to bring the trunk back after foot strike. This requires higher stimulations at high speeds where inertia effects and strike impacts are more important. While this increase trend is clearly visible for $k_{HAM,1}$, it is less obvious for k_{GLU} . On top of that, the linear approximation slope is much higher for $k_{HAM,1}$ than for k_{GLU} . This suggests that modulating k_{GLU} is not necessary to achieve gait modulation because its effect after foot strike is largely dominated by the HAM muscles. Consequently, k_{GLU} is finally kept constant for all speeds, see Table I. During the swing phase, hip flexion increases for higher speeds. So, the HFL muscles get higher stimulations (with k_{HFL} increasing) while their antagonist muscles HAM get lower stimulations (with $k_{HAM,2}$ decreasing). Under 0.45 m/s, we get a stagnation of θ_{ref} and τ and the evolution of the six parameters of interest is less obvious. Over 0.85 m/s, the

optimizer did not manage to find appropriate and robust solutions. However, co-optimizing all parameters according to the strategy described in section IV (i.e. simultaneous optimization of all parameters) could increase this range from 0.4 m/s to 0.9 m/s. These results support our linear speed control rules presented in Eq. (11).

B. Gaits comparison

Three main controllers are compared in terms of energy efficiency, trunk angle reference, stride period and stride length. These three controllers are (i) the *pure-reflex* model from [7], (ii) our CPG-based controller optimized for a single fixed speed called *fixed-CPG* and (iii) our CPG-based controller optimized to adapt the gait to a wide range of speeds called *adaptive-CPG*. All of them were optimized for target speeds ranging from 0.4 m/s to 0.9 m/s with a step of 0.05 m/s. For each target speed, five independent optimizations were performed. Contrary to the two first controllers, the *adaptive-CPG* one was optimized in a single optimization run for the whole range of speeds. These three controllers resulted in human-like gaits for the whole range of tested speeds with leg stretching and heel strikes.

All the results are presented in Fig. 3. Regarding energy efficiency (Fig. 3a), the *pure-reflex* controller and the *fixed-CPG* one perform in a similar way for speeds higher or equal to 0.5 m/s, with the *fixed-CPG* one being slightly more efficient. However, for speeds under 0.5 m/s, the *pure-reflex* controller is clearly more efficient. The main reason is that the objective function of the *fixed-CPG* also targets a good strike prediction, a constraint that is not taken into account in the *pure-reflex* optimizations. Finally, the *adaptive-CPG* model is the less energy-efficient. However, given that this model is optimized for a wide range of speeds in a single shot and not tuned for a precise gait, the small increase regarding energy-efficiency seems a reasonable price to pay.

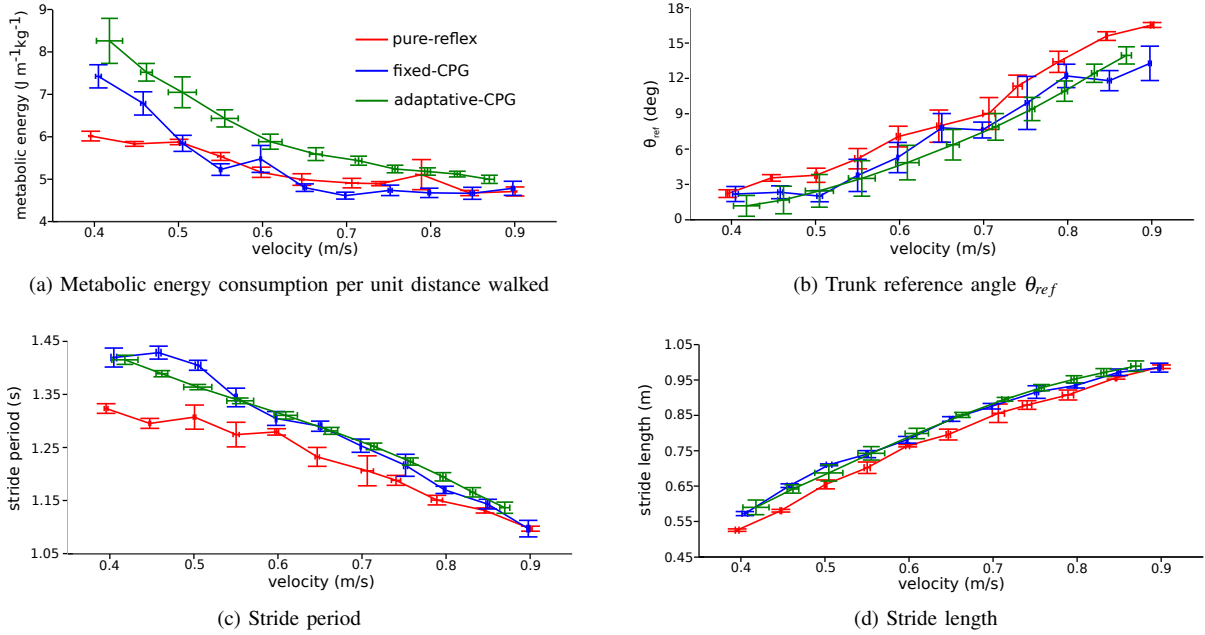


Fig. 3: We run five optimizations for each target speed with different controllers. For each set of five optimizations, the mean and the standard deviation are depicted. For graph legibility, errorbars correspond to the half of the standard deviation.

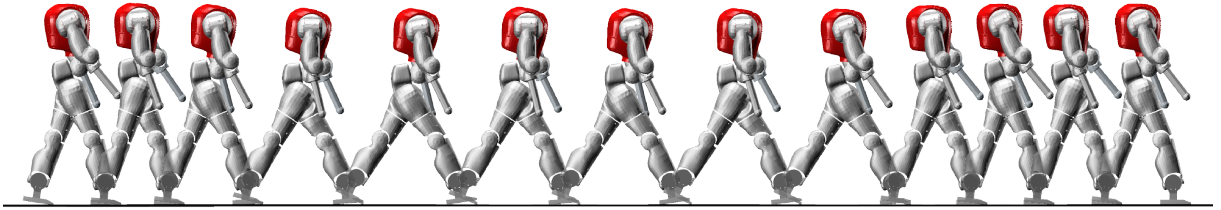


Fig. 4: COMAN is walking with its target speed increasing from 0.4 m/s to 0.9 m/s before going back to 0.4 m/s. Snapshots of the gait are taken during each double support phase to show the stride length evolution.

In terms of stride analysis (Fig. 3c and 3d), the *fixed-CPG* and the *adaptive-CPG* controllers have similar stride periods and lengths. The *pure-reflex* model, however, features lower stride periods and lengths, so favouring smaller steps with a faster frequency. Finally, another difference in gait analysis being visible in Fig. 3b is that the *pure-reflex* model also favours larger trunk tilt θ_{ref} .

C. Target speed tracking

We now focus only on the *adaptive-CPG* controllers where a wide range of speeds is optimized in a single optimization. Fig. 4 presents snapshots of the COMAN walking with its target speed increasing from 0.4 m/s to 0.9 m/s. After a few steps, it gets back its initial speed of 0.4 m/s. Fig. 5 shows a gait where we modulate the robot speed. The target speed is modified in the range from 0.4 m/s to 0.9 m/s with constant accelerations of $\pm 0.25 \text{ m/s}^2$. We measure the speed and post-process it with a 0.5 s running average, visible in green in Fig. 5. We observe that the robot is able to accelerate from 0.4 m/s to 0.9 m/s in less than 2.3 s (acceleration

of 0.22 m/s^2), so corresponding to less than two strides. In comparison, [8] requires four strides for similar accelerations while [9] targets a range of speeds nearly two times smaller once scaled to the robot height. Finally, decelerating from 0.9 m/s to 0.4 m/s is also performed in 2.3 s. Higher target accelerations do not result in higher real accelerations and might make the robot fall. During this experiment, the leg sagittal torques never exceed 30 Nm, except for the hip at high speeds (just after strike). However, these short torque peaks (less than 10% of the stride period in the worst case) never exceed the COMAN maximum hip torque of 55 Nm [16]. The reference torque signals are thus within the robot actuators capabilities. This experiment is provided as multimedia attachment.

D. Stride period prediction

The oscillators network is synchronized with feet strike using short excitation modulations (see Eq. (3)) when the oscillators prediction is too slow or too fast. During the optimization process, the objective function rewards solutions

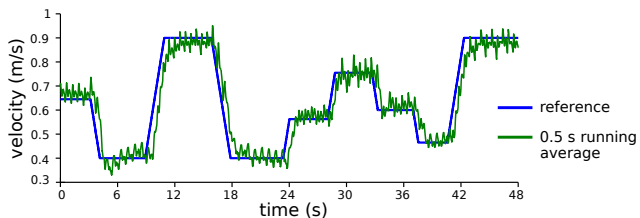


Fig. 5: The controller can track a speed reference (blue). The robot speed computed in post-process is presented in green.

minimizing these synchronization mechanisms duration, thus when the CPG correctly predicts the step period. So, these oscillators can be used to predict when the next strike will take place. This is potentially relevant to develop other mechanisms requiring synchronization with the walking gait. In Fig. 6, the robot walks at different speeds from 0.4 m/s to 0.9 m/s. For each speed, we get the stride period predicted with the oscillators structure. Then, we compare this prediction with the actual stride period. The global prediction is rather accurate. Some small differences still appear with slowest speeds: the predicted stride period is slightly higher than the actual one, revealing that the oscillators are too slow. This prediction is also presented in the multimedia attachment.

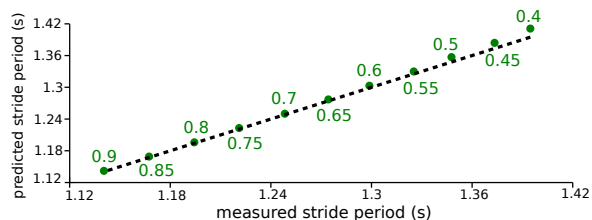


Fig. 6: The stride period predicted by the CPG is compared to the actual one for different speeds expressed in m/s (green). The dashed line corresponds to correct predictions.

E. Stepping over a hole

Since our speed modulation algorithm directly impacts the step length, it features another nice and potentially very useful property. Indeed, it can be used to temporarily alter the gait and avoid landing the foot on an undesired place like a hole. An example is provided in the multimedia attachment where a short-time speed target increase can alter the gait to perform a smaller step (likely due to the predominant frequency increase effects during the first step) followed by a longer one to cross a hole. Once this is done, the COMAN recovers its previous gait. Some snapshots of this example are provided in Fig. 7.

VI. CONCLUSION

In this contribution, we presented a bio-inspired controller able to make a humanoid robot walk over a wide range of speeds, allowing fast speed variations during the walking gait. This speed modulation was achieved using simple rules where all parameters to adapt were expressed as linear

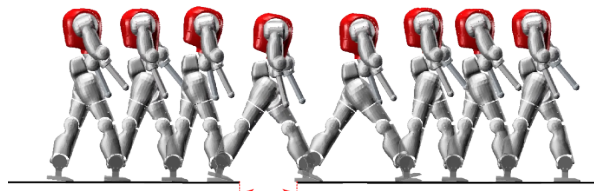


Fig. 7: COMAN gait is adapted to cross a hole before going back to its previous gait (snapshots taken during each double support phase).

functions of the target speed. Moreover, this controller, combining reflexes and a CPG in a neuromuscular model, could be tuned in one single optimization. Consequently, reflexes and CPG parameters were co-optimized to achieve a good energy-efficiency over the whole range of speeds. On top of that, the CPG could be used to predict the stride period and to modulate the gait to avoid landing the foot on unwanted locations like holes.

While the main focus of this contribution is to provide efficient walking algorithms for robots with human-like gait features, it might also help to get a better insight on human locomotion, where the existence of CPGs is still a matter open to debate. Our controller relies on Hill-type muscle models controlled by reflexes and Matsuoka oscillators, both being developed on a solid biological background. In this contribution, we demonstrated that simple modulations of the CPG frequency and amplitude, together with a trunk reference angle adaptation, could lead to large gait speeds variations and step modulation. So, like Taga [22] or Paul [23] contributions, this paper also argues that CPGs could play a major role in human locomotion, at least to modulate the gait.

However, there is still room for improvement with this controller. In particular, results are deteriorated for slow speeds in terms of energy efficiency, strike prediction and gait modulation, which is worth being investigated. Natural extensions of this controller would be to achieve 3D walking gaits, or complex obstacles avoidance. Finally, we plan to implement this controller on the real COMAN to validate our controller on real hardware.

APPENDIX A

The equations governing the firing rate x_i of each neuron N_i are presented in Eq. (9), self-inhibition equations in Eq. (10).

$$\begin{aligned}
 \dot{x}_1 &= \frac{1}{\tau} (-x_1 - \beta_A v_1 - \eta_A [x_4]^+ - \eta_D [x_2]^+ - \eta_E [x_5]^+ + u_1) \\
 \dot{x}_2 &= \frac{1}{\tau} (-x_2 - \beta_B v_2 - \eta_B [x_5]^+ - \eta_D [x_1]^+ - \eta_E [x_4]^+ + u_2) \\
 \dot{x}_3 &= \frac{1}{\tau} (-x_3 - \beta_C v_3 - \eta_C [x_6]^+ - \eta_F [x_2]^+ - \eta_G [x_5]^+ + u_3) \\
 \dot{x}_4 &= \frac{1}{\tau} (-x_4 - \beta_A v_4 - \eta_A [x_1]^+ - \eta_D [x_5]^+ - \eta_E [x_2]^+ + u_4) \\
 \dot{x}_5 &= \frac{1}{\tau} (-x_5 - \beta_B v_5 - \eta_B [x_2]^+ - \eta_D [x_4]^+ - \eta_E [x_1]^+ + u_5) \\
 \dot{x}_6 &= \frac{1}{\tau} (-x_6 - \beta_C v_6 - \eta_C [x_3]^+ - \eta_F [x_5]^+ - \eta_G [x_2]^+ + u_6)
 \end{aligned} \tag{9}$$

$$\begin{aligned}
v_1 &= \frac{1}{\gamma_A \tau} (-v_1 + [x_1]^+) & v_4 &= \frac{1}{\gamma_A \tau} (-v_4 + [x_4]^+) \\
v_2 &= \frac{1}{\gamma_B \tau} (-v_2 + [x_2]^+) & v_5 &= \frac{1}{\gamma_B \tau} (-v_5 + [x_5]^+) \\
v_3 &= \frac{1}{\gamma_C \tau} (-v_3 + [x_3]^+) & v_6 &= \frac{1}{\gamma_C \tau} (-v_6 + [x_6]^+)
\end{aligned} \quad (10)$$

APPENDIX B

Table I gathers all the optimization parameters along with their bounds. Some of these parameters are used to get the trunk angle reference θ_{ref} , the oscillator time constants τ , and the stimulations gains k_{HFL} , $k_{HAM,1}$ and $k_{HAM,2}$, according to the rules described in Appendix C.

TABLE I: Optimization parameters and their bounds

	min	max		min	max		min	max
speed			init			β		
P_θ	0.01	0.3	κ	0	0.13	β_A	4.5	6.5
P_τ	0.08	0.2	reflex			β_B	4	6
P_{HFL}	2.2	4	$S_{0,VAS}$	0.01	0.03	β_C	3	6
$P_{HAM,1}$	1.3	3.2	G_{SOL}	0.7	1.6	η		
$P_{HAM,2}$	0.5	2	G_{VAS}	0.6	20	η_A	3	6
p_θ	0	1	ϕ_{off}	2.5	π	η_B	4	7
p_τ	-0.2	0	ξ_1	0.3	10	η_C	3	6
P_{HFL}	0	4.5	ξ_2	0.004	0.15	η_D	2.5	4
$PHAM,1$	0	4.5	γ			η_E	2.5	5
$PHAM,2$	-4	0	γ_A	0.5	2.5	η_F	2.5	5
const			γ_B	0.5	2.5	η_G	3	5.5
k_{GLU}	0.8	2	γ_C	0.5	3			

APPENDIX C

The trunk angle reference θ_{ref} , the oscillator time constant τ , and the stimulations gains k_{HFL} , $k_{HAM,1}$ and $k_{HAM,2}$ are computed as simple linear functions of the target speed v_t , according to Eq. (11). v^* is an arbitrary reference speed set to 0.6 m/s. Speed modulation is then simply obtained by modifying the target speed v_t . Finally, k_{GLU} is kept constant for all speeds (see Table I).

$$\begin{aligned}
\theta_{ref} &= P_\theta + p_\theta (v_t - v^*) \\
\tau &= P_\tau + p_\tau (v_t - v^*) \\
k_{HFL} &= P_{HFL} + p_{HFL} (v_t - v^*) \\
k_{HAM,1} &= P_{HAM,1} + p_{HAM,1} (v_t - v^*) \\
k_{HAM,2} &= P_{HAM,2} + p_{HAM,2} (v_t - v^*)
\end{aligned} \quad (11)$$

REFERENCES

- [1] M. Vukobratović and B. Borovac, "Zero-Moment Point - Thirty five years of its life," *International Journal of Humanoid Robotics*, vol. 01, no. 01, pp. 157–173, Mar. 2004.
- [2] J. Chestnutt, M. Lau, G. Cheung, J. Kuffner, J. Hodgins, and T. Kanade, "Footstep Planning for the Honda ASIMO Humanoid," in *Proceedings of the 2005 IEEE International Conference on Robotics and Automation*. IEEE, 2005, pp. 629–634.
- [3] K. Kaneko, F. Kanehiro, S. Kajita, K. Yokoyama, K. Akachi, T. Kawasaki, S. Ota, and T. Isozumi, "Design of prototype humanoid robotics platform for HRP," in *IEEE/RSJ International Conference on Intelligent Robots and System*, vol. 3. IEEE, 2002, pp. 2431–2436.
- [4] H. Dallali, "Modelling and dynamic stabilization of a compliant humanoid robot, CoMan," Ph.D. dissertation, University of Manchester, 2011.
- [5] R. Kurazume, S. Tanaka, M. Yamashita, T. Hasegawa, and K. Yoneda, "Straight legged walking of a biped robot," in *2005 IEEE/RSJ International Conference on Intelligent Robots and Systems*. IEEE, 2005, pp. 337–343.

- [6] D. G. Hobbelen and M. Wisse, *Humanoid Robots: Human-like Machines*. Vienna, Austria: I-Tech Education and Publishing, 2007.
- [7] H. Geyer and H. Herr, "A muscle-reflex model that encodes principles of legged mechanics produces human walking dynamics and muscle activities," *IEEE transactions on neural systems and rehabilitation engineering : a publication of the IEEE Engineering in Medicine and Biology Society*, vol. 18, no. 3, pp. 263–73, June 2010.
- [8] S. Song and H. Geyer, "Regulating speed and generating large speed transitions in a neuromuscular human walking model," in *2012 IEEE International Conference on Robotics and Automation*. IEEE, May 2012, pp. 511–516.
- [9] F. Dzeladini, J. van den Kieboom, and A. Ijspeert, "The contribution of a central pattern generator in a reflex-based neuromuscular model," *Frontiers in Human Neuroscience*, vol. 8, June 2014.
- [10] A. J. Ijspeert, "Central pattern generators for locomotion control in animals and robots: A review," *Neural Networks*, vol. 21, no. 4, pp. 642–653, 2008.
- [11] K. Matsuoka, "Sustained oscillations generated by mutually inhibiting neurons with adaptation," *Biological Cybernetics*, vol. 52, no. 6, pp. 367–376, 1985.
- [12] —, "Mechanisms of frequency and pattern control in the neural rhythm generators," *Biological Cybernetics*, vol. 56, no. 5-6, pp. 345–353, July 1987.
- [13] R. Ronsse, D. Sternad, and P. Lefèvre, "A computational model for rhythmic and discrete movements in uni- and bimanual coordination," *Neural computation*, vol. 21, no. 5, pp. 1335–70, May 2009.
- [14] G. Pratt and M. Williamson, "Series elastic actuators," in *Proceedings 1995 IEEE/RSJ International Conference on Intelligent Robots and Systems. Human Robot Interaction and Cooperative Robots*, vol. 1. IEEE Comput. Soc. Press, 1995, pp. 399–406.
- [15] H. Dallali, M. Mosadeghzad, G. A. Medrano-Cerda, N. Docquier, P. Kormushev, N. Tsagarakis, Z. Li, and D. Caldwell, "Development of a dynamic simulator for a compliant humanoid robot based on a symbolic multibody approach," in *2013 IEEE International Conference on Mechatronics (ICM)*. IEEE, Feb. 2013, pp. 598–603.
- [16] N. G. Tsagarakis, S. Morfey, G. M. Cerda, Z. Li, and D. G. Caldwell, "COMAN a Compliant Humanoid: Optimal Joint Stiffness Tuning for Modal Frequency control," in *IEEE International Conference on Robotics and Automation. Proceedings. ICRA '13.*, 2013.
- [17] J.-C. Samin and P. Fiset, *Symbolic Modeling of Multibody Systems*. Springer, 2004.
- [18] J. M. Wang, S. R. Hamner, S. L. Delp, and V. Koltun, "Optimizing locomotion controllers using biologically-based actuators and objectives," *ACM Trans. Graph.*, p. 25, 2012.
- [19] H. Geyer, A. Seyfarth, and R. Blickhan, "Positive force feedback in bouncing gaits?" *Proceedings. Biological sciences / The Royal Society*, vol. 270, no. 1529, pp. 2173–83, Oct. 2003.
- [20] A. Schepelmann, M. D. Taylor, and H. Geyer, "Development of a Testbed for Robotic Neuromuscular Controllers," in *Robotics: Science and Systems*. MIT Press, 2012.
- [21] M. R. Dimitrijevic, Y. Gerasimenko, and M. M. Pinter, "Evidence for a spinal central pattern generator in humans." *Annals of the New York Academy of Sciences*, vol. 860, pp. 360–76, Nov. 1998.
- [22] G. Taga, "Emergence of bipedal locomotion through entrainment among the neuro-musculo-skeletal system and the environment," *Physica D: Nonlinear Phenomena*, vol. 75, no. 1-3, pp. 190–208, Aug. 1994.
- [23] C. Paul, M. Bellotti, S. Jezernik, and A. Curt, "Development of a human neuro-musculo-skeletal model for investigation of spinal cord injury," *Biol. Cybern.*, vol. 93, no. 3, pp. 153–170, Sept. 2005.
- [24] M. A. Daley, G. Felix, and A. A. Biewener, "Running stability is enhanced by a proximo-distal gradient in joint neuromechanical control." *The Journal of experimental biology*, vol. 210, no. Pt 3, pp. 383–94, Feb. 2007.
- [25] J. Kennedy and R. Eberhart, "Particle swarm optimization," in *Proceedings of ICNN'95 - International Conference on Neural Networks*, vol. 4. IEEE, 1995, pp. 1942–1948.
- [26] L. J. Bhargava, M. G. Pandy, and F. C. Anderson, "A phenomenological model for estimating metabolic energy consumption in muscle contraction," *Journal of Biomechanics*, vol. 37, no. 1, pp. 81–88, Jan. 2004.
- [27] M. P. Murray, R. C. Kory, B. H. Clarkson, and S. B. Sepic, "Comparison of free and fast speed walking patterns of normal men." *American journal of physical medicine*, vol. 45, no. 1, pp. 8–23, Feb. 1966.